Remote Detection of Chemicals with Passive Millimeter Waves[†]*

N. Gopalsami, S. Bakhtiari, T. Elmer, and A. C. Raptis
Argonne National Laboratory, Nuclear Engineering Division, Bldg. 308
9700 S. Cass Avenue, Argonne, IL 60439

September 2006

[†]Submitted to SPIE Conference on Chemical and Biological Sensors for Industrial and Environmental Monitoring, Boston, MA, October 1-4, 2006.

---

*Research supported by U.S. Department of Defense, under the U.S. Department of Energy Contract W-31-109-ENG-38.

Remote Detection of Chemicals with Passive Millimeter Waves

N. Gopalsami*, S. Bakhtiari, T. W. Elmer, and A. C. Raptis
Argonne National Laboratory, Nuclear Engineering Division, 9700 S. Cass Avenue,
Argonne, IL, USA 60439-4825

ABSTRACT

Passive millimeter-wave (mmW) systems have been used in the past to remotely map solid targets and to measure low-pressure spectral lines of stratospheric and interstellar gases; however, its application to pressure-broadened spectral detection of terrestrial gases is new. A radiative transfer model was developed to determine the detection feasibility and system requirements for passive mmW spectral detection. A Dicke-switched multispectral radiometer in the 146-154 GHz was designed and built for remote detection of stack gases. The radiometer was tested in the laboratory using a gas cell; the spectra of acetonitrile were detected passively against a cold background, which mimicked typical remote detection scenarios in the field. With Dicke-switched integration of radiometric signals, on-line calibration, and novel signal processing to minimize atmospheric fluctuation, spectral line detection of polar molecules is possible from chemical plumes a few kilometers away.

Keywords: Passive, millimeter wave, rotational spectroscopy, remote sensing, chemical plume.

1. INTRODUCTION

Active and passive spectrometers operating in the optical range have been employed in the past for a variety of environmental monitoring and remote sensing applications. Optical systems, which provide superb sensitivity as a direct consequence of high-energy vibrational transitions, are susceptible to atmospheric effects and hence are limited in range of detection. Because of longer wavelength in relation to cloud and dust particles and less atmospheric attenuation in certain frequency windows, microwaves and millimeter waves are highly suited for remote sensing applications.

Remote sensing of terrestrial targets based on radar backscattering at microwave frequencies are routinely used to monitor temporal variations of the earth's surface.[1] Spectroscopic measurement of molecular absorptions at millimeter wave frequencies have also been studied extensively in the past, primarily as laboratory-based techniques.[2-4] Passive microwave sensing and imaging of materials have also been applied in the past for special applications.[5-8] The primary application of passive mmW remote sensing has so far been dedicated to satellite and high-altitude observation of the upper atmosphere.

Because of the interaction between atoms and molecules, all materials radiate electromagnetic (EM) energy. A radiometer, which essentially is a highly sensitive receiver, can be used to detect blackbody radiation over a narrow range of the EM spectrum. With the radiation spectrum being governed by Planck's radiation law, the sensor output is a linear measure of the temperature of the scene at millimeter wavelengths. Passive sensing of EM radiation at microwave frequencies has been used in the past primarily for radioastronomical and atmospheric observations for which the sensor antenna is directed away from the surface of the earth.[9] For example, the existence of cosmic background radiation at 2.7K was discovered with a microwave radiometer in 1965. As a direct consequence of operating at longer wavelengths, millimeter waves penetrate into or originate from deeper spaces in material media. Radio frequency (RF) radiometers are generally designed to operate within atmospheric windows in the mmW bands where attenuation due to absorbing molecules such as water and oxygen in the atmosphere is low and spectral sensitivity to target molecules is high.

*gopalsami@anl.gov; phone: 1 630 252-5925; fax: 1 630 252-3250; www.anl.gov

This paper describes the modeling, design, fabrication and testing of a passive 16-channel spectrometer in the 146-154 GHz range for remote detection of chemicals. The uniqueness of the spectrometer is associated with (a) the design of its hardware to allow passive measurement of spectral lines from absorption/emission by polar molecules, (b) specially developed software for processing of multi-channel radiometric data, and (c) application of a mmW radiometric technique for terrestrial remote sensing of chemical plumes. Application of spectroscopic techniques for passive terrestrial detection of target molecules in a chemical plume at millimeter wave frequencies is a new frontier in science and the offshoots of this technology are expected in the future to have a wide range of industrial, scientific, and medical applications.

2. RADIATIVE TRANSFER MODELING

Using the relationship between the brightness and apparent temperatures, the general solution of the equation of transfer for a scatter-free atmosphere can be written as[9]

$$T_{dn}(\theta) = T_{bg} e^{-\tau(0,z)\sec(\theta)} + \sec(\theta) \int_0^\infty \kappa_a(z') T(z') e^{-\tau(0,z')\sec(\theta)} dz', \quad (1)$$

in which

$$\tau(0,z') = \int_0^{z'} \kappa_a(z) dz, \quad (2)$$

$T_{dn}(\theta)$ is the apparent temperature of the semi-infinite atmosphere observed at a zenith angle θ from ground surface, $\kappa_a(z)$ is the absorption coefficient of the atmospheric medium at height z, T_{bg} is the brightness temperatures of the background, and T(z') is kinetic temperature of the atmospheric medium at height z', respectively. Under the assumption that each layer is homogeneous, Eq. (1) reduces to

$$T_{dn}(\theta; H) = T_{bg} e^{-\tau(0,H)\sec(\theta)} + T_0 \left[1 - e^{-\tau(0,H)\sec(\theta)}\right], \quad (3)$$

in which the integration is from z=0 to z=H and the kinetic temperature $T(z)$=T_0. By modeling the atmosphere as a stratified medium made of homogeneous plane layers, Eq. (3) can be used to numerically calculate the apparent temperature of the atmosphere. Major mmW absorbing molecules in the atmosphere are water vapor and oxygen; in the frequency range of 0-300 GHz, there are water lines at 22.2 GHz and 183.3 GHz and oxygen lines at ~60 GHz (a cluster) and 118.75 GHz. The pressure-broadened absorption coefficients for these lines, for a given water vapor density, are calculated as a function of atmospheric height using the tabulated values of attenuation parameters in Ulaby *et al;*[9] oxygen concentration is assumed at 21 percent by volume.

Figure 1 depicts the geometry of the detection scenario for an upward-looking radiometer. The target cloud is assumed to be nitric oxide (NO), which emanates from a stack pipe in the form of hot gases. The absorption coefficient of NO is calculated from the Jet Propulsion Laboratory database[10] by taking into account pressure broadening. The background may be a mountain whose emissivity is less than 1. The atmosphere is divided into three layers with the target plume located in the middle layer. The emission and absorption of each layer is calculated separately and the contribution from all layers is propagated downward to determine the apparent temperature at the radiometer position. Numerical integration is performed for calculating the absorption coefficient in each layer. Using the closed form solution given by Eq. (3), contributions from the upper layer, plume, and the lower layer, respectively, can be written as

$$T_{UL}(\theta) = T_{bg} e^{-\kappa_{UL} z(h+d,H)\sec(\theta)} + T_{atm}\left[1 - e^{-\kappa_{UL} z(h+d,H)\sec(\theta)}\right] \quad (4)$$

$$T_C(\theta) = T_C\left[1 - e^{-\kappa_C z(h,h+d)\sec(\theta)}\right] \quad (5)$$

$$T_{LL}(\theta) = T_{atm}\left[1 - e^{-\kappa_{LL}\, z(0,h)\sec(\theta)}\right] \tag{6}$$

where h and d are the height and depth of the plume, H is the height of the atmosphere, and κ is the absorption coefficient for each layer. The contributions from (4) to (6) may then be combined to get the apparent temperature at the ground level using

$$T_{DN}(\theta) = T_{LL}(\theta) + \left[T_{UL}(\theta)e^{-\kappa_c z(h,h+d)\sec(\theta)} + T_C(\theta)\right]\cdot e^{-\kappa_{LL} z(0,h)\sec(\theta)}\,. \tag{7}$$

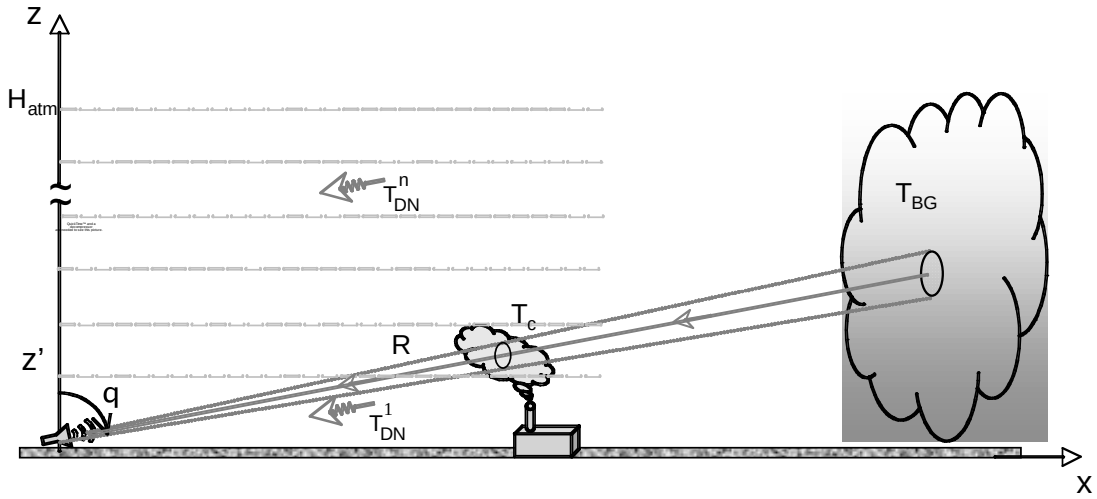

Fig. 1. Geometry of the scene used for the radiative transfer model consisting of gas plume and background within a stratified atmosphere.

Figure 2 gives the calculated absorption coefficient for standard atmosphere containing oxygen and water-vapor molecules only. Figure 3 is a plot of pressure-broadened absorption spectra of nitric oxide. To simulate the response of a Dicke-switched radiometer the apparent temperature in all cases was calculated twice, once without and once with the plume being present and the difference between the two scenes was taken as the output.

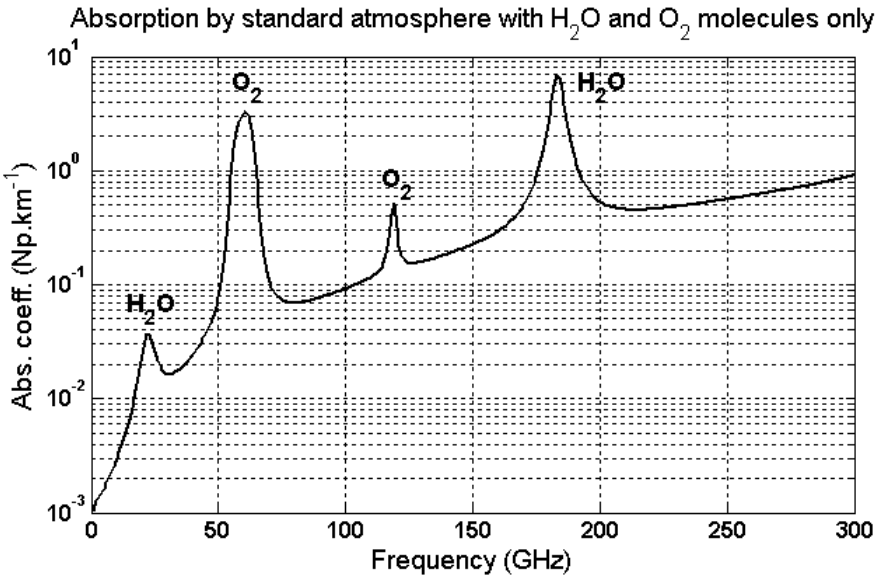

Fig. 2. Absorption coefficient for standard atmosphere as a function of frequency containing oxygen and water vapor molecules using $\theta=0^o$, H=2.5 km, T_0=288.15 K, and V_{H20}=7.5 g.m^{-3}.

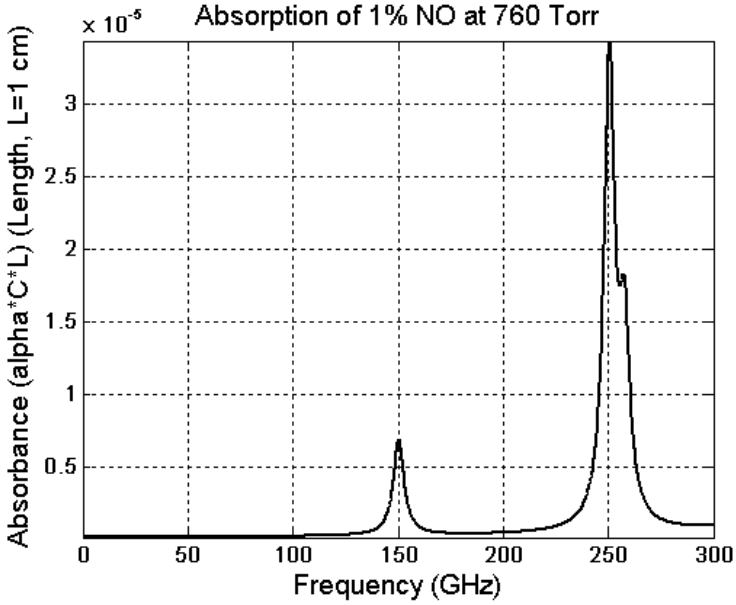

Fig. 3. Pressure-broadened absorption spectra of NO; the results are for 1% by volume of the molecule at 760 Torr.

Figure 4 shows the effect of distance to background on the radiometric temperature. For the results shown here the distance to the plume is kept constant while the distance to the background increases from 5 km to 10 km. Although the differential temperature at both peak absorption frequencies go down at larger background distances, the peak at the higher frequency ($\approx$ 250 GHz) attenuates more strongly than the one at lower frequency ($\approx$ 150 GHz).

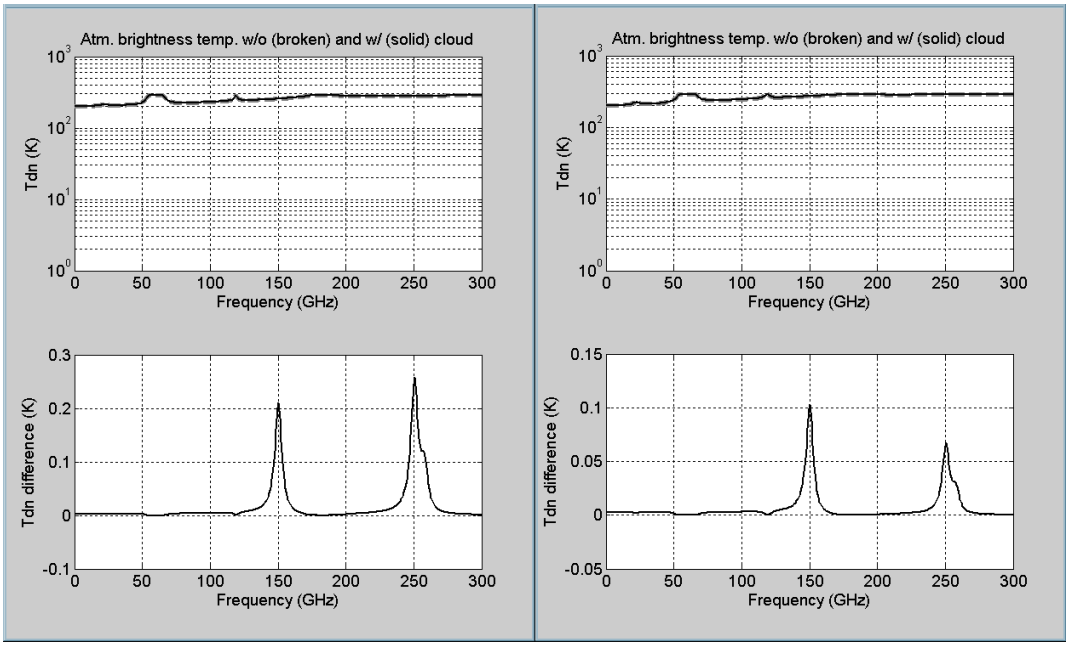

(a) $\theta = 84.3^o$, $R_c = 1.0$ km, $R_{bg} = 5.0$ km (b) $\theta = 84.3^o$, $R_c = 1$ km, $R_{bg} = 10$ km

Fig. 4. Apparent temperature as a function of frequency and for different distance to background, keeping the target distance constant. Both the absolute temperature with and without the plume (top) and the difference temperature (bottom) are displayed. For all case here $h_c = 0.1$ km, $d_c = 0.01$ km, $T_c = 288.15$ K, e =0.7 and with 1% by volume of NO. The zenith angle, radial distance to plume, and radial distance to background are shown below each plot.

The effect of plume and background temperatures on the downward-emitted radiation is also examined. Figure 5 shows the estimated peak values of radiometric temperature for plume temperatures of T_c=300 K and T_c= 450 K, respectively. As expected, the rise in the temperature of the plume results in higher emission and thus an increase in the temperature contrast. The effect of concentration of the target molecules within the plume was also examined. The results show a direct relationship between the apparent temperature and the concentration of target molecules within the plume.

The modeling results show that (i) the expected change in temperature that a radiometer observes from a weakly absorbing plume such as that of NO is very small—in the order of tens of millikelvin and (ii) the observable signal for NO is stronger for the 150GHz line than for the 250GHz line, in spite of the fact that the 250 GHz line is inherently stronger than the 150 GHz line.

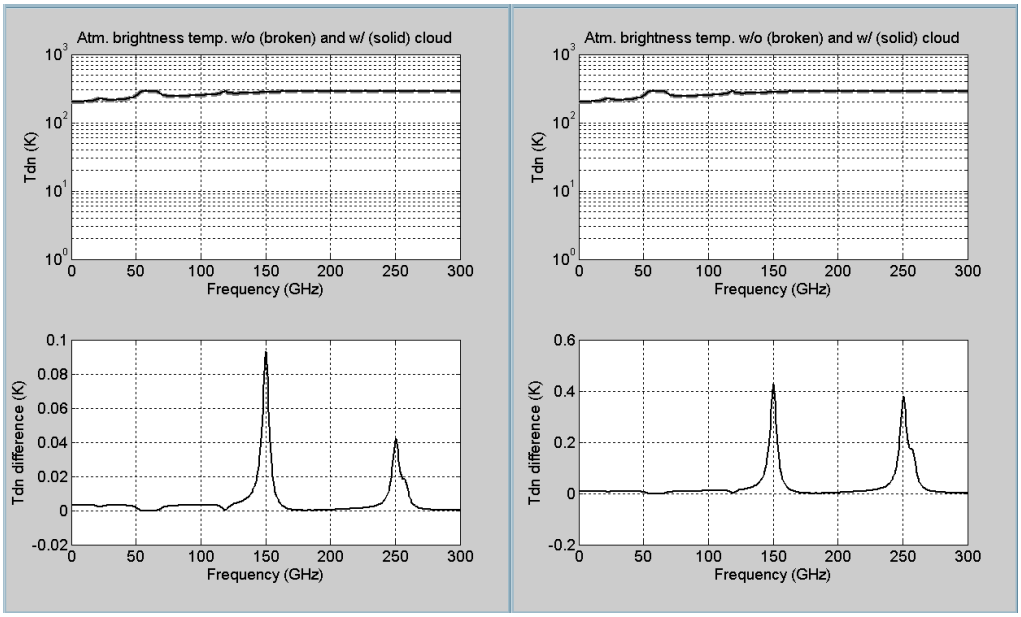

(a) T_c=300 K, R_c=5.0 km, R_{bg}=10.0 km (b) T_c=450 K, R_c=5.0 km, R_{bg}=10.0 km

Fig. 5. Apparent temperature as a function of frequency and for different plume temperatures. Both the absolute temperature with and without the plume (top) and the difference temperature (bottom) are displayed. For all cases here h_c=0.1 km, d_c=0.01 km, e=0.7 and NO at 1% by volume. Plume temperature, radial distance to plume, and radial distance to background are shown below each plot.

3. DESIGN AND FABRICATION OF RADIOMETER

A 16-channel radiometer, covering the frequency range of 146 to 154 GHz, with 500 MHz bandwidth per channel, was designed to detect the 150GHz line of NO. To detect weak spectral signals of NO, it is necessary to use a Dcike-switching radiometer configuration with long integration times. Minimum detectable temperature, ΔT_r of a Dicke-switched radiometer is given by:

$$\Delta T_r = \frac{2(T_A + T_R)}{\sqrt{B\tau}}, \tag{8}$$

where T_A is the antenna temperature, T_R the receiver noise temperature, B the predetection bandwidth, and τ the integration time. Detection sensitivities can be calculated using Eq. (8) for different radiometer configurations: uncooled, cooled, and low-noise amplifier (LNA) front ends. Based on vendor quotations, a single side band noise figure of 11.9 dB was assumed for the receiver without LNA and a noise figure of 3.2 dB for the LNA configuration. Note that LNA at 150 GHz range is still not commercially available, but can be custom built with InP-based HEMT MMIC technology. Table 1 projects the achievable detection sensitivities for the three configurations with two predetection bandwidths of 500 MHz (16 channel) and 2 GHz (4 channel). Results indicate the feasibility of achieving tens of millikelvin sensitivity with 10 min integration.

Table 1. Radiometer Performance Prediction.

Variable	Uncooled		Cooled to 77K		LNA	
	Predetection BW		Predetection BW		Predetection BW	
	500 MHz	2 GHz	500 MHz	2 GHz	500 MHz	2 GHz
Receiver Noise Figure (dB)	11.9	11.9	11.9	11.9	3.2	3.2
System temperature, K	4492	4492	1406	1406	608	608
Detection sensitivity (mK) for 10 min integration	16.4	8.2	5.2	2.6	2.2	1.1

A multispectral radiometer system consisting of the mmW front-end assembly, back-end electronics, and data acquisition hardware and software was assembled as shown in Fig. 6. A superheterodyne receiver at the front-end converts the mmW frequencies within the pass band (146-154 GHz) of the low-pass filter down to intermediate frequency (IF) range of 10-18 GHz, which subsequently goes through first-stage amplification. The back-end unit further amplifies the IF signal by passing it through another two stages of amplification. A two-stage power divider splits the signal into sixteen channels, which then goes through a bank of sixteen bandpass filters (500 MHz BW) and is subsequently down-converted to video frequency range. Each video amplifier has a Schottky barrier diode detector. To allow the radiometer to operate in Dickie-switched mode, an optical chopper was installed in front of the antenna unit, which provides a trigger signal for separating of the scene and reference signals. The outputs of the radiometer and the synchronization TTL signal from the optical chopper are all fed to an 18-bit data acquisition (DAQ) board for processing. Data collection and integration of the signals are performed using a LabVIEW program.

The efficacy of long integration times to reduce measurement uncertainty was tested next. Figure 7 gives the measured performance characteristics of individual channels. The single sideband noise figure of various channels is between 10 and 12 dB. The output signals of the channels for a uniform liquid nitrogen load are different due to gain variations and must be normalized periodically during tests. As expected, measurement uncertainty (the rms variation of the signal) decreases linearly with the square root of integration time.

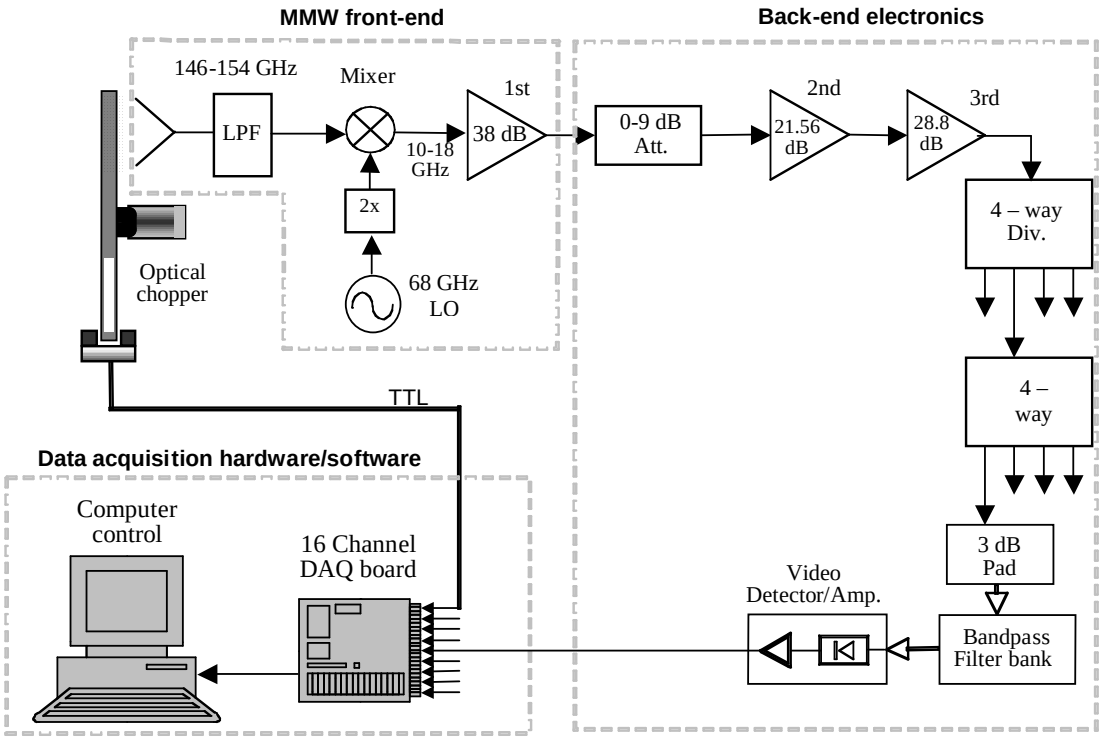

Fig. 6. Schematic diagram of sixteen channel passive mmW spectrometer showing the RF front-end, back-end electronics encompassing the filter bank, and data acquisition hardware/ software.

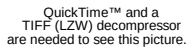

Fig. 7. Measured performance characteristics: (a) noise figure, (b) channel voltage variation to a liquid nitrogen load, and (c) rms deviation of the voltage with integration time.

4. PROOF OF PRINCIPLE TESTING

To test the proof of principle of passive MMW spectroscopy, several experiments were conducted by using chemicals with known absorption lines. The laboratory setup for the measurement of emission spectra at millimeter wavelengths is shown in Fig. 8. It mimics the detection scenario in the field, i.e., the radiometer receives the emission signals from a gas in a transparent cell against a thermally contrasting background. Instead of a hot gas against an ambient temperature object in the field scenario, we use here an ambient temperature gas against a cold background. Measurement was made with a 30 second integration time and

over a ~30 minute time span. The normalized radiometer response for a hot load (time interval between 0 and ~5min.), a human hand (time intervals centered at ~7 min. and ~15 min.), and CH_3CN vapor (centered at ~10 min. and ~20 min.) is given in Fig. 9 (a). While all channels show the same normalized response for uniform loads such as the hot load and hand, the response pattern changes when CH_3CN is introduced into the cell according to its emission spectra. The frequency response of the channels for CH_3CN is shown in Fig. 9 (b) corresponding to a time instant marked by a vertical line in Fig. 9 (a); the channel numbers 15-0 correspond to 146.25-153.75 GHz in 0.5 GHz intervals.

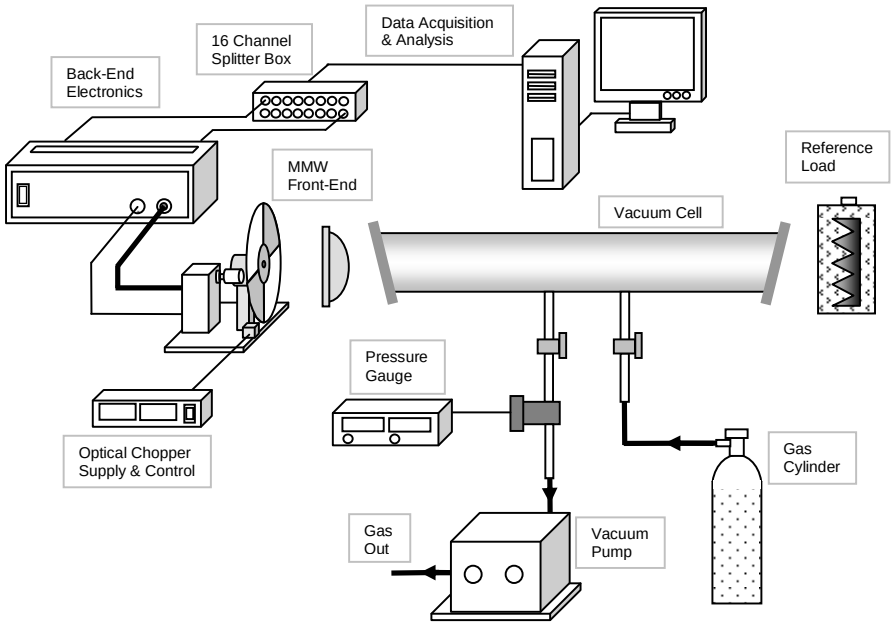

Fig. 8. Laboratory setup for passive measurement of emission spectra of gases at millimeter wavelengths.

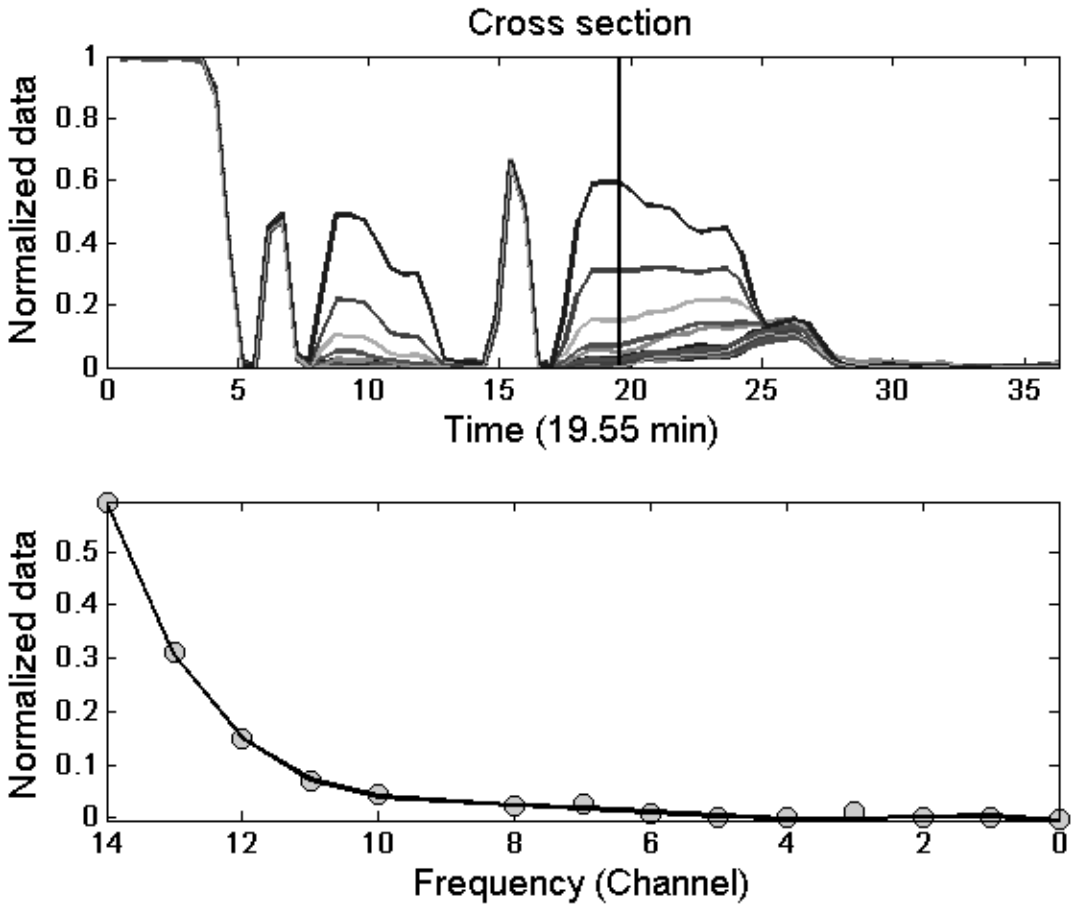

Fig. 9. Display of laboratory measurement results for CH_3CN gas at various pressures: (a) radiometer output from 15 channels displayed as normalized linear traces as a function of time and (b) frequency spectra at a given instant in time marked by the vertical line in (a).

Because the rotational spectra of CH_3CN are known and can be obtained from molecular spectral databases such as that of the Jet Propulsion Laboratory, we can calculate its emission spectra for a temperature difference of 223K and compare it with the measured spectrum. Figure 10 gives the calculated and measured emission spectra for 5% CH_3CN at 1Torr. While the agreement is fairly good at high signal (emission) levels, the channel fluctuations become obvious at low signal levels. It shows that extreme care must be taken to bring down these uncertainties by frequent calibration, channel normalization, signal integration, and baseline subtraction.

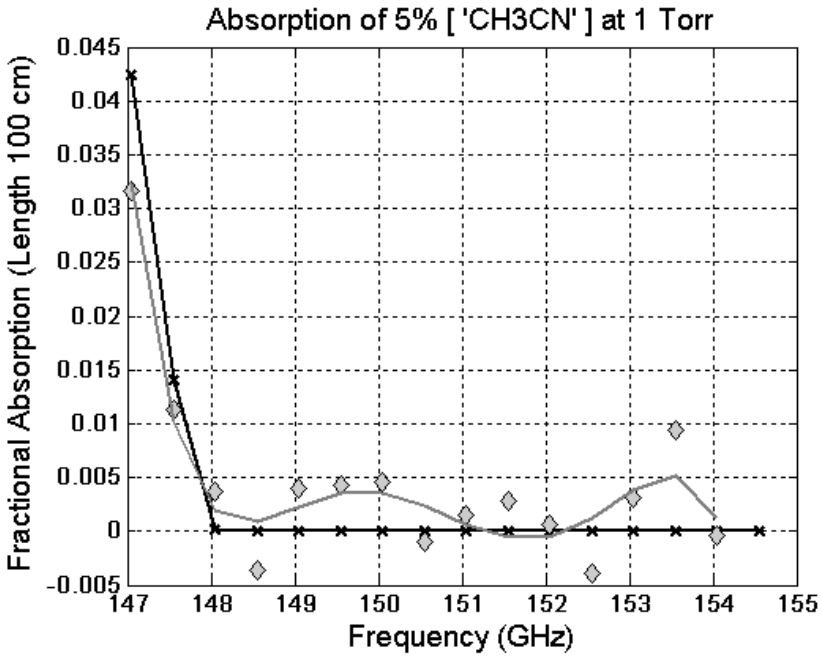

Fig. 10. Comparison of measured and simulated spectra for 5% CH_3CN.

The next step in our development is to prepare the system for field testing and to develop signal processing schemes to compensate for atmospheric fluctuation. The front end will be kept at constant temperature by a thermoelectric cooler; this will minimize the drift of the channel gains. A 12-inch lens antenna will be mounted in front of the radiometer such that the far field radiation from the scene is focused into the scalar horn of the radiometer. A pointing telescope will be mounted in parallel to the lens axis so that the radiometer lens antenna can be aimed at the plume; a radio beacon at 150 GHz will be used to further refine the alignment between the lens and the telescope. The entire radiometer assembly will be mounted on rotational and tilting platforms to align along azimuth and elevation.

5. CONCLUSIONS

We have designed and developed a remote sensing radiometer for spectroscopic detection of airborne chemicals from a facility's stack. A radiative transfer model was developed to simulate the expected radiometric signals in a typical remote sensing scenario consisting of a ground-based radiometer aiming at a hot nitric oxide plume with a mountain background behind it. The simulation results show the feasibility of detecting the weak 150GHz spectral line of nitric oxide from a few kilometers away using a state-of-the-art radiometer with a long integration time. A Dicke-switched radiometer was built to measure the spectral power between 146 and 154 GHz using 16 channels with 500 MHz bandwidth per channel. The proof of principle was tested in the laboratory by passively measuring the spectral lines of CH_3CN vapor in a gas cell against the background of a liquid nitrogen load. The measured spectra agreed with the calculated spectra of CH_3CN. The radiative modeling of typical remote sensing scenarios and the laboratory measurements of CH_3CN spectra with our multispectral radiometer show that it is feasible to remotely detect airborne chemicals passively with millimeter waves. Care must, however, be exercised in developing appropriate baseline subtraction and signal processing techniques in detecting weak spectral lines against fluctuating atmosphere.

ACKNOWLEDGMENTS

The authors wish to acknowledge the United States Air Force for the financial support of this project. They also wish to thank Haruko Murakami of University of California Berkeley and Ronald N Lanham of Argonne for their technical assistance.

REFERENCES

1. S. Bakhtiari and R. Zoughi, "Backscattering Characteristics of Tall Prairie Grass Canopies at Microwave Frequencies: A Theoretical Approach," *Remote Sensing of Environment*, vol. 36, no. 2, pp. 137-147, May 1991.
2. N. Gopalsami, S. Bakhtiari, A. C. Raptis, S. L. Dieckman, and F. C. DeLucia, "Millimeter-Wave Measurements of Molecular Spectra with Application to Environmental Monitoring," *IEEE Trans. on Inst. and Meas.*, vol. 45, No. 1, 1996.
3. N. Gopalsami, A. C. Raptis, and J. Meier, "Millimeter-Wave Cavity Ringdown Spectroscopy," *Review of Scientific Instruments*, vol. 73, pp. 259-262, 2002.
4. N. Gopalsami and A. C. Raptis, "Millimeter-Wave Radar Sensing of Airborne Chemicals," *IEEE Trans. Microwave Theory Techniques*, Vol. 49, pp. 646-653, 2001.
5. S. Bakhtiari, and R. Zoughi, "Thickness Measurement of Lossy Multi-Layered Dielectric Medium Backed by A Conducting Plate Using Incoherent Reflectivity at Microwave Frequencies," *Rev. of Prog. in QNDE*, vol. 10, Plenum Press, New York, 1991.
6. F.T. Ulaby, R. K. Moore, and A. K. Fung, *Microwave Remote Sensing: Active and Passive, Vol. I—Microwave Remote sensing Fundamentals and Radiometry*, Addison-Wesley, Reading, MA, 1981.
7. L. Yujiri, M. Shouri, and P. Moffa, “Passive Millimeter-Wave Imaging,” *IEEE Microwave Magazine*, September 2003.
8. N. Gopalsami and A. C. Raptis, “Millimeter-Wave Imaging of Thermal and Chemical Signatures,” Proc. of the Conf. on Passive Millimeter-Wave Imaging Technology III, ed. R. M. Smith, SPIE, vol. 3703, pp. 130-138, 1999.
9. M. A. Janssen (Ed.), *Atmospheric Remote Sensing by Microwave Radiometry*, John Wiley and Sons, New York, 1993.
10. R. L. Poynter and H. M. Pickett, *Submillimeter, Millimeter, and Microwave Spectral Line Catalog*, Jet Propulsion Lab., Pasadena, CA, vol. 80-23, 1983.